Structural and Electronic Properties of Poly(9,9-dialkylfluorene)-Based Alternating Copolymers in Solution: An NMR Spectroscopy and Density Functional Theory Study

ARTICLE *in* THE JOURNAL OF PHYSICAL CHEMISTRY C · JULY 2013

Impact Factor: 4.77 · DOI: 10.1021/jp4062576

9 AUTHORS, INCLUDING:

M. Luísa Ramos
University of Coimbra
62 PUBLICATIONS **721** CITATIONS
SEE PROFILE

Ana Charas
Institute of Telecommunications
67 PUBLICATIONS **1,020** CITATIONS
SEE PROFILE

Ullrich Scherf
Bergische Universität Wuppertal
680 PUBLICATIONS **21,656** CITATIONS
SEE PROFILE

Hugh D Burrows
University of Coimbra
421 PUBLICATIONS **6,300** CITATIONS
SEE PROFILE

THE JOURNAL OF PHYSICAL CHEMISTRY C

Article

pubs.acs.org/JPCC

Structural and Electronic Properties of Poly(9,9-dialkylfluorene)-Based Alternating Copolymers in Solution: An NMR Spectroscopy and Density Functional Theory Study

Licínia L. G. Justino,*[,†,‡] M. Luísa Ramos,[†,‡] P. E. Abreu,[†] Ana Charas,[§] Jorge Morgado,[§,∥] Ullrich Scherf,[⊥] Boris F. Minaev,[#] Hans Ågren,[▽] and Hugh D. Burrows[†]

[†]Departamento de Química, Faculdade de Ciências e Tecnologia, Universidade de Coimbra, 3004-535 Coimbra, Portugal

[‡]Centro de Neurociências e Biologia Celular, Faculdade de Ciências e Tecnologia, Universidade de Coimbra, 3004-517 Coimbra, Portugal

[§]Instituto de Telecomunicações, and [∥]Department of Bioengineering, Instituto Superior Técnico, Universidade Técnica de Lisboa, Avenida Rovisco Pais, P-1049-001 Lisboa, Portugal

[⊥]Makromolekulare Chemie, Bergische Universitat Wuppertal, D-42097 Wuppertal, Germany

[#]Department of Natural Sciences, Bogdan Khmelnitskij National University, 18031 Cherkasy, Ukraine

[▽]Department of Theoretical Chemistry, Royal Institute of Technology, S-106 91 Stockholm, Sweden

ABSTRACT: The structural and electronic properties of three alternating poly(9,9-dialkylfluorene) copolymers, poly[2,7-(9,9-bis(octyl)-fluorene)-*alt*-benzothiadiazole] (F8BT), poly[2,7-(9,9-bis(2′-ethylhexyl)-fluorene)-*alt*-thiophene *S*,*S*-dioxide] (PFTSO2), and poly[2,7-(9,9-bis(2′-ethylhexyl)-fluorene)-*alt*-1,4-phenylene] (PFP), containing, respectively, benzothiadiazole (BT), thiophene *S*,*S*-dioxide, and phenylene groups, have been investigated and compared to those of the homopolymer poly[2,7-(9,9-bis(2′-ethylhexyl)-fluorene)] (PF2/6). The NMR spectra and corresponding shielding tensors of the ^{1}H and ^{13}C nuclei have been studied in solution and are interpreted by density functional theory (DFT) with complete geometry optimization using the B3LYP functional. Particular emphasis is placed on the conformational behavior and electronic properties in the electronic ground state. In addition, time-dependent DFT is applied to obtain detailed insight into the character of selected excited states. A new TDDFT interpretation is presented for optical absorption spectra of singlet and triplet states that have previously been reported for these fluorene-based conjugated copolymers using photoexcitation and pulse radiolysis-energy transfer studies. As well as providing detailed assignment of excited states, the results show that the triplet excitation is slightly more localized than S_1 excitation, in agreement with experimental observations. The DFT analysis provides a link between structure and NMR, optical, electronic properties, allowing optimization of the potential of such polymers for photovoltaic and electroluminescence applications.

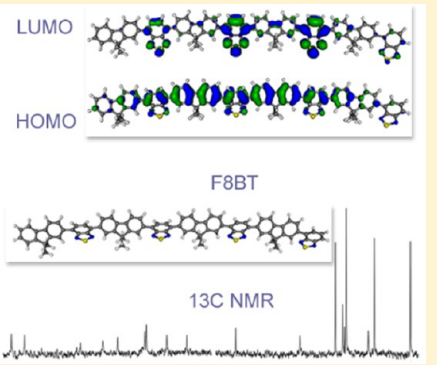

INTRODUCTION

Conjugated organic polymers constitute a class of technologically important materials that are progressively opening the way to substitute or augment technologies in electronics and optoelectronics based on inorganic semiconductors by their homologues based on cheaper and more easily processed organic compounds. Conjugated organic polymers are finding applications in light emitting diodes (LEDs), thin-film transistors, sensors, photovoltaic cells,[1−3] and show potential as artificial muscles, corrosion inhibitors, electronic textiles,[4] and nerve cell communications. Poly(9,9-dialkylfluorenes) (PFs) and their copolymers are among the most important materials for application as luminescent materials in devices because of good chemical and thermal stability, blue light emission, high photoluminescence (PL) and fluorescence quantum efficiency, and possibilities of tuning emission to wavelengths spanning the entire visible spectrum, either by copolymerization or by energy transfer.[5−8]

The performance of either light emitting devices or photovoltaic systems based on conjugated polymers depends on a fine balance between the injection and transport of electrons and holes and the photophysical properties of the polymer. Large injection barriers and differences in charge mobility in the polymer will hamper an efficient recombination of the electrical charges, thus compromising the electroluminescence yields. This can be minimized by the incorporation of electron-donating or electron-withdrawing moieties on the conjugated polymer backbone, which can modulate the ionization potential (IP), electron affinity (EA),

Received: June 25, 2013
Revised: July 26, 2013

   dx.doi.org/10.1021/jp4062576 | *J. Phys. Chem. C* XXXX, XXX, XXX−XXX

and energy gap. The electronic states in these systems are relatively localized, and current views suggest that they are best treated within a molecular exciton description. However, we will refer to this latter property as the band gap because of its common usage within the conjugated polymer community.

Although fluorene homopolymers have excellent luminescent properties, they are better for facilitating hole than for electron injection and transport. The inclusion of electron-accepting groups covalently linked to the polymer backbone can increase electron affinity, thus improving electron injection and transport. Groups such as thiophene and ethynylene can rectify charge imbalance by enhancing electron transport.[8] In contrast, the high hole injection barriers of polyfluorenes can be lowered by inclusion of electron-donating units, such as carbazole[9,10] or alkoxy substituents.[11] These groups can either be incorporated within the main polymer chain in alternating or random copolymers or used as end-caps. This will affect polymer conformation, which will be important in understanding electron delocalization between fluorene and the other groups. In this Article, structural studies based on multinuclear NMR spectroscopy and theoretical calculations using density functional theory (DFT) and time-dependent DFT (TDDFT) are applied to structures and electronic properties of alternating fluorene-based copolymers, with particular emphasis on conformational effects and excited-state behavior. The NMR shielding tensor at a nucleus is characteristic of the electron distribution, making this a sensitive method for studying the electronic structure of a given molecule. Complete electronic spectral and photophysical properties have previously been reported for these fluorene-based conjugated copolymers.[12,13] Quantum mechanical electronic structure analysis provides a link between the structure and these electronic and optoelectronic properties, allowing their rationalization for existing materials, while also suggesting routes to new materials with enhanced characteristics. Additionally, the structural parameters obtained from quantum mechanical calculations provide valuable information on the structures of the polymers, which are difficult to obtain by X-ray diffraction or electron diffraction due to problems in producing single crystals. DFT is particularly useful for the study of the geometry and energetics of organic molecules because it includes electron correlation at a relatively low computational cost. In addition, time-dependent DFT has provided a valuable route for studying transient species, such as triplet states[14] and charged species,[15] of fluorene-based polymers.

The structural and electronic properties of three alternating PF copolymers, poly[2,7-(9,9-bis(octyl)-fluorene)-*alt*-benzothiadiazole] (F8BT), poly[2,7-(9,9-bis(2′-ethylhexyl)-fluorene)-*alt*-thiophene *S*,*S*-dioxide] (PFTSO2), and poly[2,7-(9,9-bis(2′-ethylhexyl)-fluorene)-*alt*-1,4-phenylene] (PFP), which have, respectively, the benzothiadiazole (BT), thiophene *S*,*S*-dioxide, and phenylene groups, will be studied and compared to those of the homopolymer poly[2,7-(9,9-bis(2′-ethylhexyl)-fluorene)] (PF2/6). In addition, time-dependent DFT (TDDFT) is used to obtain detailed insights into the character of the excited singlet and triplet states.

EXPERIMENTAL METHODS

Reagents. The synthesis of PF2/6 has been described previously.[16] The synthesis and characterization of PFP, PFTSO2, and F8BT are reported elsewhere.[12,13] Chloroform-*d* (99,8 atom % ^{2}H) was purchased from Sigma-Aldrich, Inc., Germany. All other compounds were of the purest grade available and were used without further treatment.

NMR Methodology. PF2/6, PFP, F8BT, and PFTSO2 samples were prepared by dissolving a weighed amount of the polymer in chloroform-*d* and were kept protected from light; all molar concentrations are given in terms of polymer repeat units. Chloroform is known to be a good solvent for polyfluorenes[7] and is chosen to minimize the aggregation seen in aromatic solvents, such as toluene.[17,18] The ^{1}H and ^{13}C NMR spectra were recorded on a Varian UNITY-500 NMR spectrometer (at 499.824 and 125.692 MHz, respectively). The residual ^{1}H signal of $CDCl_3$ (δ = 7.27 ppm) and the ^{13}C triplet centered at δ = 77.2 ppm, relative to TMS, were used as internal references for ^{1}H and for ^{13}C, respectively.

Computational Details. For the ground (S_0) state studies, the molecular optimizations were performed by DFT without symmetry constrains using the GAMESS[19] code. The calculations employed the B3LYP (Becke three-parameter Lee−Yang−Parr) exchange correlation functional, which combines the hybrid exchange functional of Becke[20] with the correlation functional of Lee, Yang, and Parr (LYP).[21] The structures of F2/6 oligomers n = 1−3 were optimized using the 3-21G* and 6-31G** basis sets. The results indicate that there are no significant differences between the structures obtained at the two calculation levels, and, consequently, we have chosen the 3-21G* basis sets to optimize the oligomers n = 1−4 of F2/6, PFP, F8BT, and PFTSO2 (the alkyl chains at the C-9 positions were replaced by methyl groups to reduce the computation time). At the final equilibrium geometries with minimum energy, the maximum gradients were 10^{-5} hartree bohr^{-1} for the monomers, dimers, and trimers and 2×10^{-4} for the tetramers. The ionization potentials, electron affinities, and HOMO−LUMO gaps of the polymers were obtained by employing the reciprocal rule for polymers, which states that many electronic properties of homopolymers tend to vary linearly as functions of the reciprocal of chain length.[22] For some oligomers, simulation of the ^{13}C NMR spectra was performed to validate the theoretical geometrical parameters. The nuclear shieldings were computed at the B3LYP/GIAO (gauge-including atomic orbital method) level using the 6-31G** basis sets. The NMR calculations were carried out with the NWCHEM[23] program employing a fine integration grid (FINE option). ^{13}C and ^{1}H relative chemical shifts (δ) are given with respect to the absolute shielding values (σ) of tetramethylsilane (TMS) obtained at the same computational level ($\sigma = \sigma_{ref} - \sigma$).

For the excited-state studies, the TDDFT (B3LYP/6-31G**) method is used in the framework of the Dalton code.[24,25] Linear response in TDDFT approach is used for the vertical singlet−singlet ($S_0 \rightarrow S_n$) and singlet−triplet ($S_0 \rightarrow T_n$) transitions. The $T_1 \rightarrow T_n$ absorption spectra are calculated by the quadratic response method starting with the S_0 optimized structure. Additional calculations are performed in the framework of the self-consistent field PM3 approximation with account of configuration interaction (CI) in a complete active space.[26] The second derivatives of the potential energy in the Born−Oppenheimer approximation with respect to all internal coordinates have been calculated, and the Hessian matrix has been diagonalized in the DFT approach. Thus, all vibrational frequencies have been determined and analyzed to check the criteria of the real equilibrium.

dx.doi.org/10.1021/jp4062576 | J. Phys. Chem. C XXXX, XXX, XXX−XXX

RESULTS AND DISCUSSION

NMR Characterization. Figure 1 shows the structures of the homopolymer PF2/6 and of the copolymers PFP, F8BT, and PFTSO2. We will start by studying their conformations in solution using NMR, a very powerful analytical tool that is very sensitive to the electronic structure of the molecules. Additionally, it may also give information on delocalization of charge between the copolymer repeat units on the backbone, because this will affect the electronic density and ring currents. Figures 2 and 3 present, respectively, the ^{1}H and ^{13}C NMR spectra of the polymers and include the attribution of the resonances of PF2/6 and F8BT. The NMR parameters are summarized in Table 1.

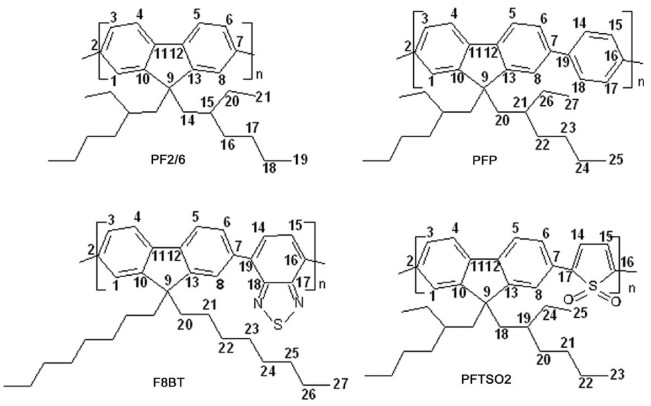

Figure 1. Chemical structures of PF2/6, PFP, F8BT, and PFTSO2.

The ^{1}H NMR spectra of PF2/6, PFP, and PFTSO2 show approximately the same groups of resonances in the alkyl chain region due to the 2-ethylhexyl side chain, while F8BT shows the peaks typical of octyl side chain. Because the alkyl chain regions of PFP and PFTSO2 are very similar to that of PF2/6, we can easily assign the most upfield two resonances to the 2-ethylhexyl CH_3 protons and the broad signals around 1 and 2.15 ppm to the CH_2 resonances. The strong signal observed around 1.55 ppm is due to the presence of residual water, probably coming from the solvent. Two small unidentified signals are observed around 1.26 ppm in PFP, F8BT, and PFTSO2 and around 2.2 ppm in PF2/6 and F8BT. These are very sharp resonances and are probably impurities, such as trace solvents and grease.

Comparing the aromatic regions, we see that the chemical shifts of the fluorene units, that is, of protons 1/8, 3/6, and 4/5, of PF2/6 (7.64−7.83 ppm), PFP (7.68−7.84 ppm), and PFTSO2 (resonances at 7.65 and 7.84 ppm) are all very similar. In contrast, the chemical shifts of the fluorene unit in F8BT show a strong downfield shift (7.96−8.12 ppm) as compared to the other three copolymers and PF8 in the same solvent (7.71−7.88;[28] which excludes the octyl side chain from being the cause of the downfield shift). The usual downfield shifts in ^{1}H signals in aromatic systems are explained through the ring current model,[29−31] according to which, if there is an external magnetic field that is perpendicular to the molecular plane, ring currents will be induced in the mobile π electrons, which will diminish (increase) the out-of-plane component (σ_{zz}) of the magnetic shielding tensor ($\sigma_{av} = (\sigma_{xx} + \sigma_{yy} + \sigma_{zz})/3$) of the ring protons in diatropic (paratropic) systems. However, the σ_{zz} component of the magnetic shielding tensor is not available from solution NMR. The observable solution NMR isotropic chemical shift, δ

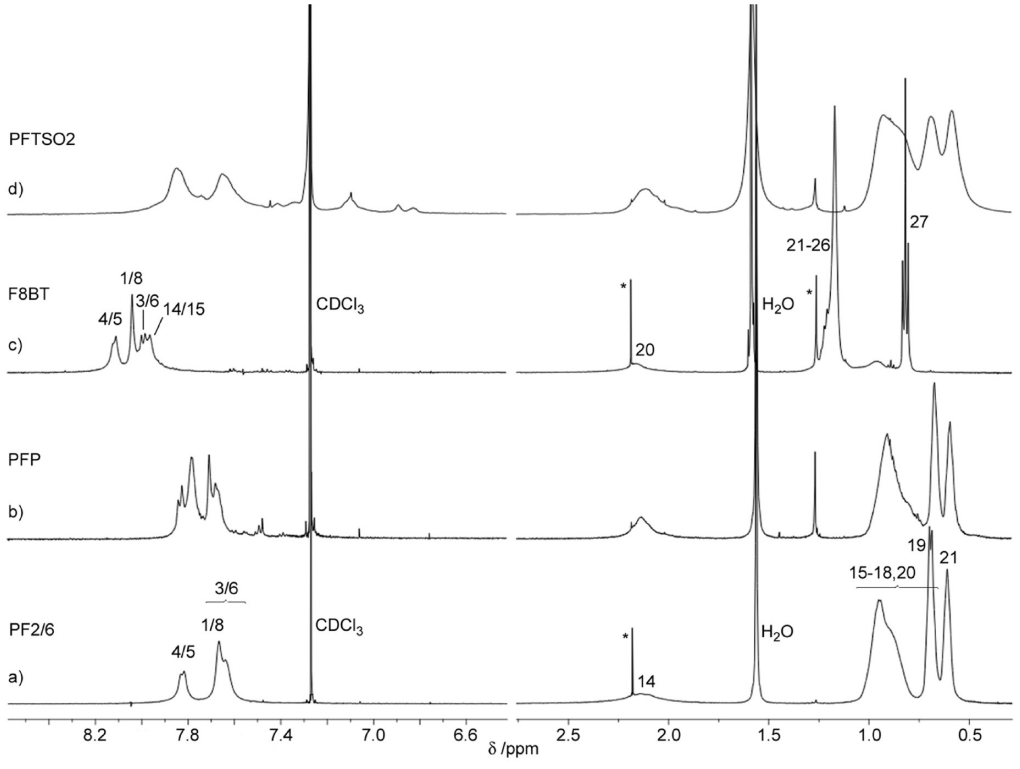

Figure 2. ^{1}H NMR spectra of the poly(9,9-diakylfluorene)s in $CDCl_3$ at 298 K: (a) PF2/6 (0.010 M); (b) PFP (0.008 M); (c) F8BT (0.005 M); (d) PFTSO2 (0.003 M). Attribution of the PF2/6 and F8BT ^{1}H resonances was established previously.[27] Unidentified signals possibly due to impurities, such as trace solvents and grease, are indicated with "*".

dx.doi.org/10.1021/jp4062576 | J. Phys. Chem. C XXXX, XXX, XXX−XXX

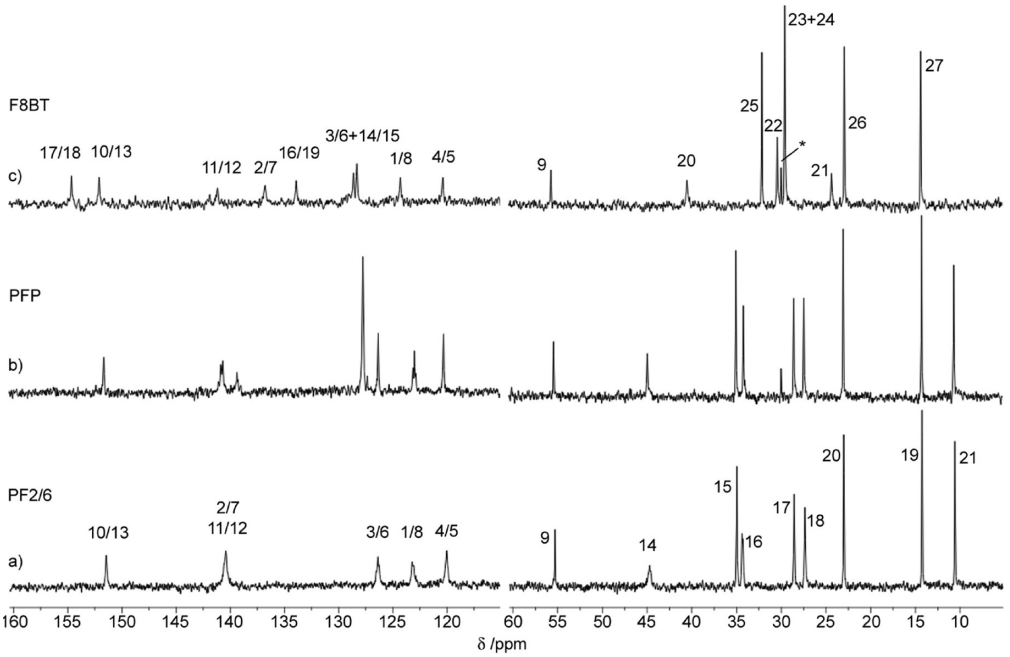

Figure 3. ^{13}C NMR spectra of the poly(9,9-diakylfluorene)s in $CDCl_3$ at 298 K: (a) PF2/6 (0.010 M); (b) PFP (0.008 M); (c) F8BT (0.005 M). Attribution of PF2/6 and F8BT ^{13}C resonances was established previously.[27,28] Unidentified signals possibly due to impurities, such as trace solvents and grease, are indicated with "*".

Table 1. Experimental ^1H and ^{13}C NMR Chemical Shifts of PF2/6, PFP, F8BT, and PFTSO2 in $CDCl_3$ Solution at 298 K

PF2/6		PFP		F8BT		PFTSO2
^1H	^{13}C	^1H	^{13}C	^1H	^{13}C	^1H
			Aromatic			
7.83	151.45	7.84	151.60	8.12	154.58	7.84
7.82	140.42	7.82	140.62	8.11	152.01	7.83(s)
7.67	126.37	7.78	139.30	8.04	141.09	7.74(w)
7.64	123.21	7.77	127.68	8.00	136.70	7.65
	120.03	7.71	126.26	7.98	133.83	7.48(w)
		7.68	122.92	7.97	128.55	7.41(w)
		7.68(s)[a]	120.23	7.96	128.22	7.34(w,+)[a]
					124.23	7.09(+)
					120.28	6.89(w)
						6.83(w)
			Pseudoaromatic			
	55.30		55.35		55.66	
			Alkylic			
2.18(*)[a]	44.72	2.18(*)	44.87	2.18(*)	40.45	2.18(b)
2.14(b)[a]	34.97	2.13(b)	34.97	2.16(b)	32.07	1.58
1.55	34.39	1.56	34.13	1.58	30.35	1.26(*)
0.95(b)	28.56	1.26(*)	29.92(*)	1.26(*)	29.92	0.93(b)
0.94(b)	27.35	0.90(b)	28.50	1.20(s)	29.52	0.89(s)
0.90(s)[a]	23.01	0.89(s)	27.38	1.17	29.49	0.85(s)
0.70	14.27	0.88(s)	22.99	0.96(b)	24.28	0.68
0.69	10.59	0.67	14.21		22.85	0.58
0.61		0.59	10.61	0.83	14.32	
				0.81		
				0.80		

[a]"b", "w", "s", "+", and "*" stand for broad, weak, shoulder, several shoulders, and unidentified, respectively.

$= \sigma_{av}(TMS) - \sigma_{av}$, is an orientationally averaged quantity because of molecular tumbling and the nonplanarity of the backbones of the polymers. This includes contributions from the in-plane components of the magnetic shielding tensor, which are not dependent to any major extent on the π-ring currents. This means that the isotropic chemical shift is not a quantitative measure of the π-ring currents. However, it is a qualitative measure, and, as discussed elsewhere,[32] enhanced downfield shifts are an indication of the presence of π-ring currents, which suggests in our case a greater degree of π

dx.doi.org/10.1021/jp4062576 | J. Phys. Chem. C XXXX, XXX, XXX−XXX

Table 2. Comparison of Selected Interatomic Distances (r, in angstroms) and Dihedral Angles (Φ, in deg) for the DFT Optimized Structures of F2/6 Oligomers n = 1−3[a]

	3-21G*	6-31G**		3-21G*	6-31G**
n = 1			n = 3		
r(1,2)	1.402	1.400	r(1,2)	1.403	1.401
r(1,10)	1.389	1.390	r(1,10)	1.390	1.391
r(2,3)	1.400	1.399	r(2,3)	1.399	1.399
r(3,4)	1.399	1.397	r(3,4)	1.398	1.396
r(4,11)	1.396	1.397	r(4,11)	1.395	1.396
r(9,10)	1.535	1.529	r(9,10)	1.537	1.531
r(10,11)	1.413	1.410	r(10,11)	1.412	1.409
r(11,12)	1.475	1.470	r(11,12)	1.472	1.466
r(12,13)	1.414	1.410	r(12,13)	1.412	1.409
Φ(10,11,12,13)	0.0	0.0	r(7,2a)	1.487	1.484
			r(1a,2a)	1.411	1.410
n = 2			r(1a,10a)	1.386	1.388
r(1,2)	1.402	1.400	r(2a,3a)	1.409	1.409
r(1,10)	1.389	1.391	r(3a,4a)	1.395	1.393
r(2,3)	1.400	1.399	r(4a,11a)	1.395	1.396
r(3,4)	1.400	1.397	r(9a,10a)	1.536	1.531
r(4,11)	1.396	1.397	r(10a,11a)	1.413	1.410
r(9,10)	1.534	1.529	r(11a,12a)	1.469	1.464
r(10,11)	1.414	1.410	r(12a,13b)	1.413	1.410
r(11,12)	1.475	1.468	r(7a,2b)	1.487	1.484
r(12,13)	1.413	1.410	r(1b,2b)	1.412	1.411
r(7,2a)	1.487	1.484	r(1b,10b)	1.386	1.388
r(1a,2a)	1.410	1.410	r(2b,3b)	1.410	1.409
r(1a,10a)	1.385	1.387	r(3b,4b)	1.395	1.393
r(2a,3a)	1.408	1.409	r(4b,11b)	1.395	1.396
r(3a,4a)	1.397	1.395	r(9b,10b)	1.535	1.530
r(4a,11a)	1.397	1.397	r(10b,11b)	1.413	1.410
r(9a,10a)	1.533	1.528	r(11b,12b)	1.473	1.467
r(10a,11a)	1.413	1.409	r(12b,13b)	1.413	1.410
r(11a,12a)	1.475	1.468	Φ(10,11,12,13)	−0.4	−0.1
r(12a,13a)	1.415	1.411	Φ(6,7,2a,3a)	40.2	37.2
Φ(10,11,12,13)	0.5	0.5	Φ(10a,11a,12a,13a)	−0.1	0.1
Φ(6,7,2a,3a)	46.1	40.1	Φ(6a,7a,2b,3b)	34.4	33.5
Φ(10a,11a,12a,13a)	0.9	0.7	Φ(10b,11b,12b,13b)	−0.3	−0.1

[a]The atom labeling is given in Figure 1.

delocalization from the benzothiadiazole unit into the F8BT backbone. For PFP and PFTSO2, however, we cannot rule out the occurrence of significant electron delocalization from the copolymer repeat units because cancellation may occur between the different contributions to σ_{av}.

In the ^{13}C NMR spectra, the alkyl chain region of PFP is similar to that of PF2/6, because both have ethylhexyl side chains, and the PFP resonances can be attributed based on the previous attribution in PF2/6.[27] In the aromatic region of the PFP spectrum, the signals with lower intensities correspond reasonably well with the fluorene resonances of PF2/6, while the large signal at 127.68 ppm is due to the 14/15 and 17/18 carbons of PFP. For F8BT, small downfield shifts are observed for all of the fluorene ^{13}C resonances, except that for the 2/7 atoms, again suggesting a significant degree of delocalization from the BT unit. These downfield shifts are explained through a decrease in the average difference in energy between the ground state and all excited states of the molecule, ΔE, caused by the delocalization of charge from the BT unit (the paramagnetic contribution, $\sigma_p \propto -(1/\Delta E)$, is dominant for the ^{13}C chemical shifts).

No significant shifts of the fluorene resonances are observed in the ^{13}C spectrum of PFP. The ^{13}C NMR spectrum of PFTSO2 was not run due to lack of material, but is not important for the present discussion. The ^{13}C resonances are relatively sharp, suggesting that the polymers are dissolved at the molecular level in the range of concentrations considered in this study. This is supported by previous small-angle X-ray (SAXS), neutron scattering (SANS), and fluorescence studies.[17,28] As discussed previously,[28] the spectral line-widths at half-height of the alkylic ^{13}C resonances are mainly explained by the effect of the spin−spin relaxation times.

Theoretical Studies on Structural and Electronic Properties. As discussed above, fluorenes are the precursors of a variety of important copolymers. Copolymerization of fluorenes with electron-accepting or electron-withdrawing units affords polymers with better charge transport, and thus better device properties. F8BT and PFTSO2 copolymers contain, respectively, the 2,1,3-benzothiadiazole and thiophene S,S-dioxide units, electron-withdrawing moieties that we expect will improve electron-accepting properties with respect to PF2/6. PFP contains a phenylene repeat unit, which, in principle, will only have a small effect on the electronic properties of PF2/6.

dx.doi.org/10.1021/jp4062576 | J. Phys. Chem. C XXXX, XXX, XXX−XXX

We will start by calculating the ground-state structural and electronic properties of the n = 1−4 oligomers of F8BT, PFTSO2, PFP, and PF2/6 at the DFT level. DFT, and in particular the B3LYP functional, has been widely used in the study of the geometries and energetics of conjugated polymers, and extensive studies have proved its importance.[19,27,28] Because the computation of the tetramers using large basis sets is extremely time-consuming, we started by comparing the results obtained using the 6-31G** and the 3-21G* basis sets for the n = 1−3 oligomers of F2/6, to check for significant differences in the computed geometries. Because it has been shown that the substitution of the alkyl side chains at position 9 of the five membered rings by methyl groups does not significantly affect the equilibrium geometries[33] or the molecular orbital distribution,[34] we have taken this procedure to reduce the computational time. Table 2 compares the structural parameters using the two basis sets. We can see that there are no significant differences at the two levels of calculation, with the differences in bond lengths varying from 0.000 to 0.007 Å and with an average difference of 1.2° in torsion angles.

To further validate the use of the 3-21G* basis sets for calculating the geometries, we have simulated the ^{13}C NMR chemical shifts for the optimized geometries of some oligomers of F2/6, PFP, and F8BT and have compared these spectra to the experimental NMR spectra of the polymers in $CDCl_3$ solution (only the aromatic regions are compared because we have omitted the alkyl chains from the calculations). NMR is sensitive to very small electronic changes, and thus the calculation of NMR parameters is a very stringent test of the electronic structure. Consequently, the comparison between theoretical and experimental chemical shifts can be used as a tool for evaluating how close are the theoretical structures (here we refer to the repeat unit structure) to the actual structures in solution, and to what extent these can be used to predict the electronic properties. This is most important when there are no solid-state structural parameters available to compare with the calculated structures. The ^{13}C chemical shifts of the oligomers were calculated at the GIAO/B3LYP/6-31G** level[27] and are shown in Figure 4. Although the theoretical spectra were calculated for the static equilibrium geometry of the monomer or dimer in the gas phase and the experimental spectra were obtained for the polymers in solution at room temperature (that is, in the calculation rovibrational and zero-point energy effects, intermolecular interactions, including solvent, and the actual size of the system in solution, are not taken into account), we can see that there is in general very good agreement between the theoretical and the experimental spectra, validating the use of the 3-21G* basis set. This validation indicates that the theoretical gas-phase B3LYP/3-21G* structures can be used to describe the solution structures (in terms of repeat units). A further relevant aspect is that the energetic stabilization that occurs through conjugation with the increase in oligomer size is shown by the calculated spectra for F2/6 oligomers when going from the monomer to the dimer and is seen through the decreasing upfield trend of the calculated chemical shifts relative to the experimental shifts of PF2/6 (Figure 4a). This is expected because the NMR shielding constant depends on $-1/\Delta E$, where ΔE is the average difference in energy between the ground state and all excited states of the molecule. The systematic smaller δ values observed for all of the calculated spectra relative to the experimental polymer spectra must be partly explained by this factor.

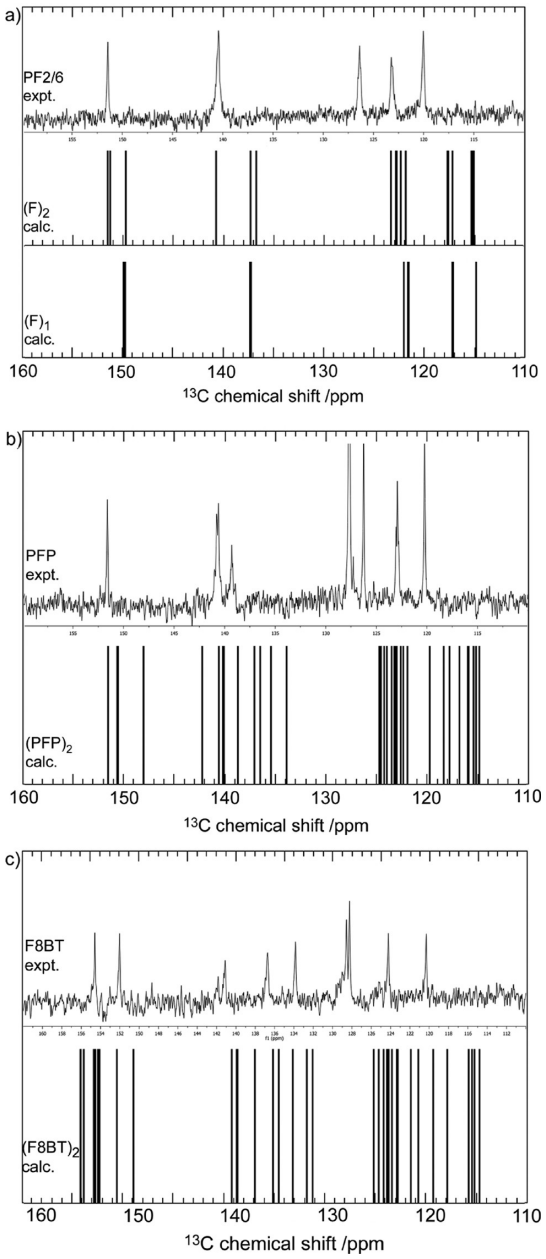

Figure 4. Calculated and experimental ^{13}C NMR spectra (aromatic region) of (a) PF2/6, (b) PFP, and (c) F8BT (in the calculated spectra the intensities are arbitrary). See details of the experimental spectra in the caption of Figure 3.

The above conclusions increase our confidence in the use of the theoretical B3LYP/3-21G* structures to predict the electronic properties of the polymers. Figure 5 shows the B3LYP/3-21G* optimized geometries of the PFTSO2 n = 1 to n = 4 oligomers, and Figure 6 presents the geometries of $(F2/6)_4$, $(PFP)_4$, $(F8BT)_4$, and $(PFTSO2)_4$. Tables 3 and 4 report selected geometrical parameters for the oligomers. The interunit torsion angles vary from 33.5° to 46.1° in the $(F2/6)_n$ series, from 30.6° to 54.8° in the $(PFP)_n$ series, from 27.3° to 36.2° for $(F8BT)_n$, and from 24.0° to 32.4° for the $(PFTSO2)_n$ oligomers. The interunit bond lengths, identified as $r(7,2)$, $r(7,19)$, $r(16,2)$, and $r(7,17)$, depending on the polymer, are 1.487 Å for the $(F2/6)_n$ oligomers, vary from 1.487 to 1.490

dx.doi.org/10.1021/jp4062576 | J. Phys. Chem. C XXXX, XXX, XXX−XXX

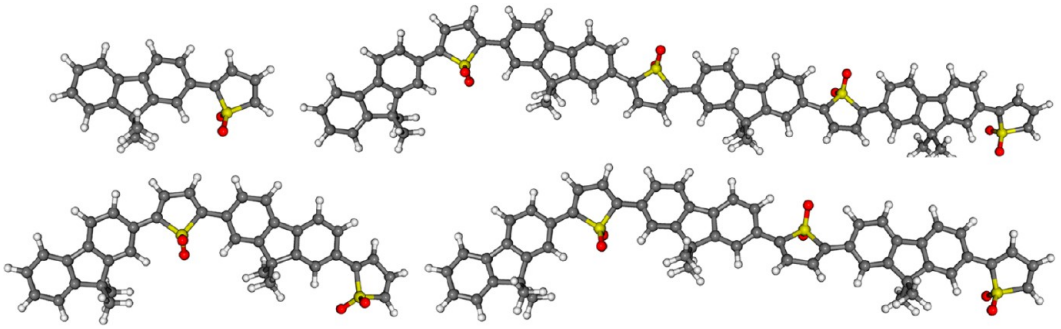

Figure 5. Optimized structures (B3LYP/3-21G*) of the $(PFTSO2)_n$ (n = 1−4) oligomers.

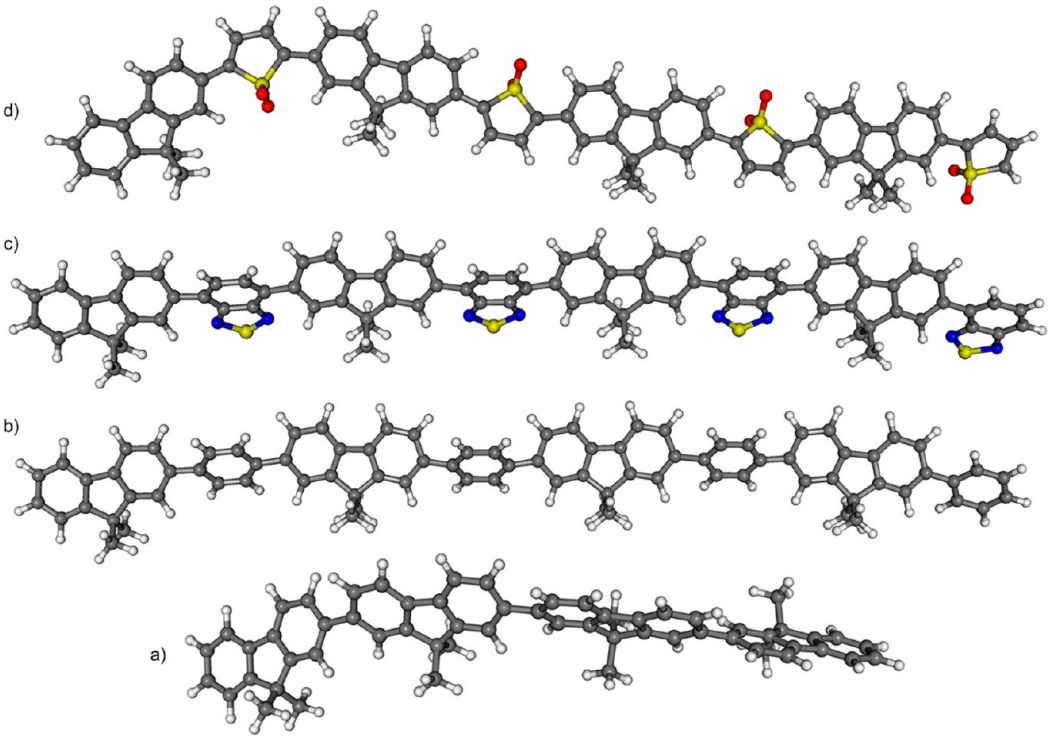

Figure 6. Optimized structures (B3LYP/3-21G*) of the (a) $(F2/6)_4$, (b) $(PFP)_4$, (c) $(F8BT)_4$, and (d) $(PFTSO2)_4$ oligomers.

Å in the $(PFP)_n$ series, vary from 1.480 to 1.484 Å for $(F8BT)_n$ oligomers, and vary from 1.455 to 1.458 Å for $(PFTSO2)_n$. We can see that both the interunit torsion angles and the interunit bond lengths are significantly smaller for the F8BT and PFTSO2 oligomers relative to F2/6 and PFP oligomers. The more planar conformations and the shorter bond lengths for F8BT and PFTSO2 indicate that there is a higher degree of electronic conjugation between the fluorene moieties and the end-caps in these two polymers. The five-membered ring of fluorene is almost planar in all of the oligomers (Φ-(10,11,12,13) varies from 0.0° to 1.1°). $(F2/6)_4$ adopts a helix conformation, while in the other tetramers the fluorene units twist randomly. In the PFTSO2 trimer and tetramer, the conformation adopted seems to be that which minimizes the electric dipole moment of the molecule. We can also conclude that the geometrical parameters do not change to a significant amount in each series of oligomers, which suggests that we can study the properties of the polymers from the results obtained for the oligomers.

We will now consider some of the electronic properties of the polymers from the results obtained for their oligomers. Figures 7−10 show the HOMO and LUMO orbitals for the $(F2/6)_n$, $(PFP)_n$, $(F8BT)_n$, and $(PFTSO2)_n$ oligomers, respectively, and Figure 11 compares the LUMOs of the tetramers. In F2/6 and PFP oligomers, both the HOMO and the LUMO are spread over the conjugated backbone. However, for F8BT and PFTSO2 oligomers, the LUMOs are mainly localized on the benzothiadiazole and thiophene *S*,*S*-dioxide groups due to the presence of the electronegative sulfur and oxygen atoms. This result suggests that in these two polymers the benzothiadiazole and thiophene *S*,*S*-dioxide groups act as electron acceptors, and we can anticipate that these polymers will have higher electron affinities than PF2/6 and PFP. Because PFs usually have better hole- than electron-accepting and transport properties, this will improve the balance in charge transport.

Figures 12a and b shows the evolution of the energies of the HOMO and LUMO orbitals and of the HOMO−LUMO gap, respectively, as a function of the reciprocal of the chain length $(1/n)$ for the four polymers. As expected for π-conjugated systems,[22] the energies of the frontier orbitals vary linearly with $1/n$, and the HOMO−LUMO gap decreases as the size of the

dx.doi.org/10.1021/jp4062576 | J. Phys. Chem. C XXXX, XXX, XXX−XXX

Table 3. Selected Interatomic Distances (angstroms) and Dihedral Angles (deg) in the Optimized Structures of $(F2/6)_n$ and $(PFP)_n$ Oligomers (n = 1−4) Calculated at the B3LYP/3-21G* Level

	n = 1	n = 2	n = 3	n = 4
$(F2/6)_n$				
r(11,12)	1.475	1.475	1.472	1.472
r(11a,12a)		1.475	1.469	1.470
r(11b,12b)			1.473	1.469
r(11c,12c)				1.472
r(7,2a)		1.487	1.487	1.487
r(7a,2b)			1.487	1.487
r(7b,2c)				1.487
Φ(10,11,12,13)	0.0	0.5	−0.4	−0.2
Φ(10a,11a,12a,13a)		0.9	−0.1	−0.4
Φ(10b,11b,12b,13b)			−0.3	−0.2
Φ(10c,11c,12c,13c)				−0.4
Φ(6,7,2a,3a)		46.1	40.2	39.3
Φ(6a,7a,2b,3b)			34.4	33.5
Φ(6b,7b,2c,3c)				40.0
$(PFP)_n$				
r(11,12)	1.472	1.472	1.472	1.472
r(11a,12a)		1.471	1.467	1.468
r(11b,12b)			1.468	1.468
r(11c,12c)				1.467
r(7,19)		1.487	1.487	1.487
r(7a,19a)		1.489	1.488	1.488
r(7b,19b)			1.488	1.490
r(7c,19c)				1.488
r(16,2a)		1.487	1.488	1.487
r(16a,2b)			1.488	1.488
r(16b,2c)				1.489
Φ(10,11,12,13)	0.1	0.1	−0.1	0.1
Φ(10a,11a,12a,13a)		−0.2	−0.1	−0.2
Φ(10b,11b,12b,13b)			0.2	−0.5
Φ(10c,11c,12c,13c)				−1.1
Φ(6,7,19,14)	−42.3	−42.2	39.8	39.1
Φ(6a,7a,19a,14a)		−44.3	−40.3	−39.7
Φ(6b,7b,19b,14b)			−43.8	−54.8
Φ(6c,7c,19c,14c)				−41.9
Φ(15,16,2a,3a)		41.6	−41.3	−41.9
Φ(15a,16a,2b,3b)			48.2	46.3
Φ(15b,16b,2c,3c)				30.6

oligomer increases. The energies of the frontier orbitals, the HOMO−LUMO gaps, and the vertical ionization potentials and electron affinities are summarized in Table 5. The values presented for the polymers (n = ∞) were obtained by extrapolating the number of monomer units to infinity.

Considering the data in Table 5, we see that F8BT and PFTSO2 have the highest electron affinities (EAs), 2.15 and 2.38 eV, respectively, of the four polymers. This means that the copolymerization with the electron-accepting benzothiadiazole and thiophene *S*,*S*-dioxide groups decreases the energy of the LUMO orbitals, improving the electron-accepting properties for the copolymers. In contrast, incorporation of the phenylene group has a negligible effect, just decreasing the electron injection barrier by 0.04 eV. Comparing the ionization potentials, we can see that the hole injection barriers increase slightly for all of the copolymers (the IP_v is 5.67 eV for PF2/6, 5.73 eV for PFP, 5.56 eV for F8BT, and 5.80 eV for PFTSO2). In conclusion, and not surprisingly, the copolymerization with the phenylene group does not significantly affect the properties with respect to PF2/6, although it may have effects on morphology and film formation. However, for F8BT and PFTSO2, despite a slight increase in the IP_v of PFTSO2 (0.13 eV), the electron-accepting properties are markedly improved (by 1.24 eV for F8BT and by 1.47 eV for PFTSO2), indicating that these copolymers should have better device properties in terms of electron injection. IP_v and EA_v values calculated by DFT usually differ from the experimental values by around 20%, due to factors such as the neglect of solvent or solid-state interactions and limitations of the presently available exchange correlation functionals, as discussed in ref 35. However, these authors have shown that this does not affect the qualitative trends in either IP_v or EA_v.[35]

Time-Dependent DFT Studies of Excited-State Properties. *Singlet−Singlet Absorption Spectra.* Before analysis of the spectra and structure of the oligomers of the PFP polymer, we will consider the properties of the monomer. The highest occupied molecular orbital (HOMO) and lowest unoccupied molecular orbital (LUMO) of the monomer $(PFP)_1$ are shown in Figure 8. One can see that the LUMO includes a combination of bonding orbitals for the C−C chemical bonds oriented in the long axis direction, while the HOMO includes a combination of bonding orbitals for C−C chemical bonds oriented along the short axis. From TDDFT calculations, it is found that the first excited triplet (T_1) and singlet (S_1) states are mostly HOMO−LUMO in nature. Thus, upon the $S_0 \rightarrow S_1$ transition, the electron π cloud produces a kind of rotation inside the molecular plane. Because of this particular symmetry of the HOMO−LUMO structure, the first absorption and emission bands are very intense. For the same reason, the optimized geometry of these excited states differs from that of the ground state. The lowest S and T states, which are of $\pi\pi^*$ type, embrace the whole conjugation chain except the saturated $C(CH_3)_2$ group on the five carbon atom ring. Although the $(PFP)_1$ monomer is a nonsymmetrical species, the HOMO and LUMO wave functions are close to a_2 and b_1 irreducible representations of the C_{2v} point group, respectively (considering the π-plane of the four rings as the yz-plane, and the z-axis as bisecting the 5−6 bond). Thus, the $S_0 \rightarrow S_1$ transition moment is polarized along the y axis (b_2) and includes very large contributions from the terminus atoms (opposite sign products of the wave functions). The $S_0 \rightarrow S_1$ transition in $(PFP)_1$ at 4.2 eV (Table 6) provides the only intense absorption band (f = 1.096) in the visible region; the next intense band is predicted to be in the UV region (λ = 236 nm, f = 0.55).

The transient absorption spectra observed with pulse radiolysis of argon-saturated benzene solutions of polyfluorene copolymers in the presence of triplet energy donors are similar to the spectra obtained by flash photolysis; thus they are attributed to $T_1 \rightarrow T_n$ absorption.[12]

Calculations of the $T_1 \rightarrow T_n$ absorption spectra have been carried out by quadratic response TDDFT method, starting from the optimized ground-state structure.[24,25] The T_1 state has been generated by linear response TDDFT, and all excited T_n states have been calculated as quadratic response from the T_1 density. The control calculations made by linear response TDDFT method provided very similar results.

The T_1 state in all studied cases is mostly the HOMO−LUMO excitation, which comprises the whole molecule. The orbital structure of the T_1 state is quite similar to that of the S_1 state analogues. A minor difference is a slightly larger

dx.doi.org/10.1021/jp4062576 | J. Phys. Chem. C XXXX, XXX, XXX−XXX

Table 4. Selected Interatomic Distances (angstroms) and Dihedral Angles (deg) in the Optimized Structures of $(F8BT)_n$ and $(PFTSO_2)_n$ Oligomers (n = 1−4) Calculated at the B3LYP/3-21G* Level

	n = 1	n = 2	n = 3	n = 4
$(F8BT)_n$				
r(11,12)	1.472	1.471	1.470	1.471
r(11a,12a)		1.467	1.463	1.463
r(11b,12b)			1.466	1.462
r(11c,12c)				1.468
r(7,19)	1.483	1.482	1.480	1.481
r(7a,19a)		1.483	1.482	1.481
r(7b,19b)			1.484	1.482
r(7c,19c)				1.482
r(16,2a)		1.481	1.482	1.481
r(16a,2b)			1.481	1.480
r(16b,2c)				1.481
Φ(10,11,12,13)	−0.6	0.3	0.6	0.6
Φ(10a,11a,12a,13a)		0.5	0.7	−0.6
Φ(10b,11b,12b,13b)			0.5	−0.8
Φ(10c,11c,12c,13c)				0.4
Φ(6,7,19,14)	−33.2	−28.2	33.5	33.1
Φ(6a,7a,19a,14a)		−31.7	−27.6	33.4
Φ(6b,7b,19b,14b)			−27.9	30.1
Φ(6c,7c,19c,14c)				36.2
Φ(1S,16,2a,3a)		33.4	−27.3	−32.0
Φ(1Sa,16a,2b,3b)			33.5	−34.1
Φ(1Sb,16b,2c,3c)				−33.3
$(PFTSO2)_n$				
r(11,12)	1.471	1.471	1.470	1.471
r(11a,12a)		1.468	1.465	1.467
r(11b,12b)			1.467	1.470
r(11c,12c)				1.465
r(7,17)	1.458	1.456	1.455	1.456
r(7a,17a)		1.457	1.456	1.457
r(7b,17b)			1.456	1.455
r(7c,17c)				1.458
r(16,2a)		1.457	1.457	1.455
r(16a,2b)			1.457	1.455
r(16b,2c)				1.455
Φ(10,11,12,13)	0.5	−0.2	−0.4	−0.3
Φ(10a,11a,12a,13a)		0.2	0.7	−1.0
Φ(10b,11b,12b,13b)			0.5	−0.6
Φ(10c,11c,12c,13c)				0.3
Φ(6,7,17,14)	32.1	−28.4	24.0	−31.4
Φ(6a,7a,17a,14a)		−30.1	(153.7)[a] *−24.8*	(146.1) *−31.9*
Φ(6b,7b,17b,14b)			28.0	(148.2) *−30.6*
Φ(6c,7c,17c,14c)				32.4
Φ(1S,16,2a,3a)		26.6	−29.0	26.9
Φ(1Sa,16a,2b,3b)			(−151.1) *28.1*	(−155.4) *23.6*
Φ(1Sb,16b,2c,3c)				(−153.2) *26.4*

[a]Φ(6a,7a,17a,14a) is given in parentheses, and Φ(8a,7a,17a,14a) is given in italics.

contribution (11.4%) of the HOMO−2 → LUMO+1 excitation to the wave function of T_1 state in comparison with the contribution of the S_1 state (7.4%). The permanent dipole moment of the T_1 state (0.42 D) is similar to that in the ground state (0.36 D). For comparison, the permanent dipole moment of the S_1 state is also rather small (0.21 D). Excited-state dipole moments start to grow to about 1 D for the next S and T excitations in the range 250−240 nm; only in the high energy, far UV region (below 210 nm) can we see a number of CT states with very high dipole moments (for example, the T_7 state with an energy 6.1 eV has a dipole moment of 18.9 D).

Interpretation of the $T_1 \rightarrow T_n$ Absorption. The second excited T_2 state of the $(PFP)_1$ monomer exhibits a very low $T_1 \rightarrow T_2$ absorption intensity (f = 0.002) and has the transition energy of 0.99 eV, which is in the near IR region (1250 nm). The next $T_1 \rightarrow T_3$ transition at 452 nm (2.77 eV, Table 6) has an extremely high oscillator strength f = 2.576; its polymeric analogue is responsible for the copolymer transient absorption spectra, presented in Figure 2 of ref 12. With the increase of the copolymer chain length, the T−T transition energy falls very quickly for the first members of the series $(PFP)_2$ and $(PFP)_3$. Qualitatively it follows to the polymer limit, observed at 760

dx.doi.org/10.1021/jp4062576 | J. Phys. Chem. C XXXX, XXX, XXX−XXX

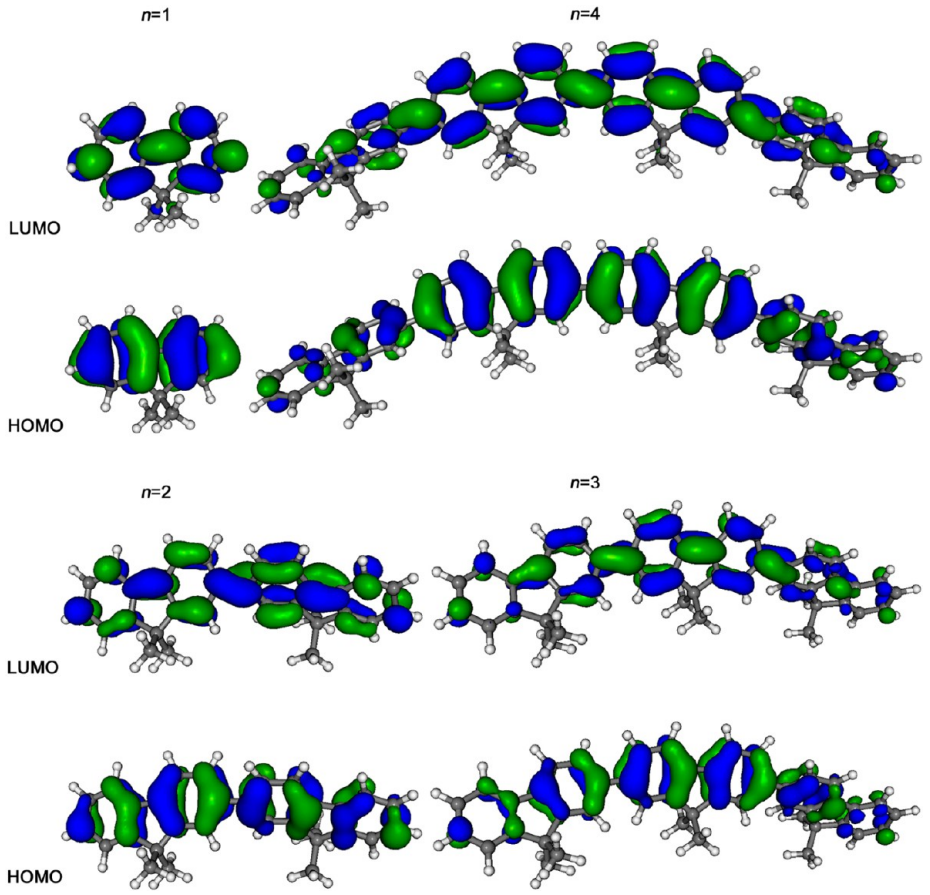

Figure 7. Contour plots of HOMO and LUMO orbitals of $(F2/6)_n$ (n = 1−4) oligomers.

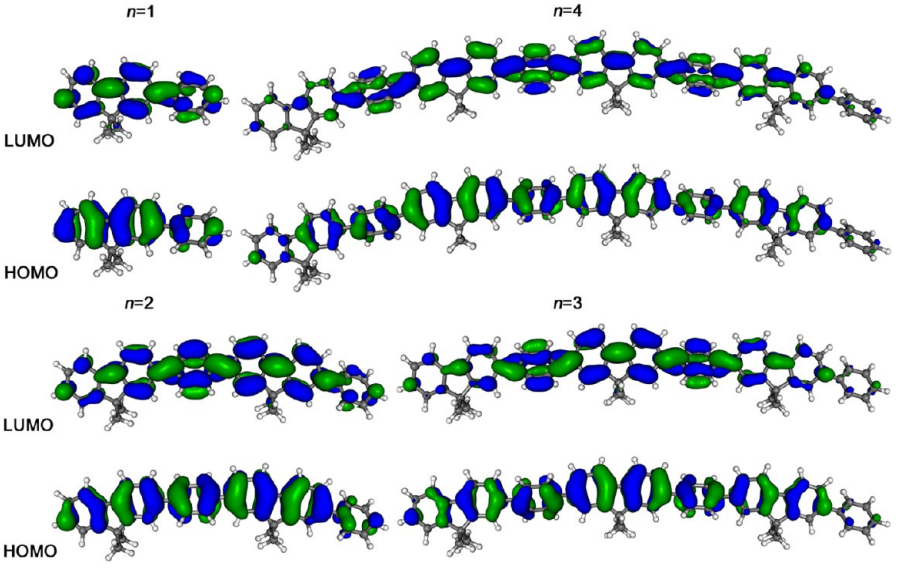

Figure 8. Contour plots of HOMO and LUMO orbitals of $(PFP)_n$ (n = 1−4) oligomers.

nm (1.7 eV).[12] To understand the orbital nature and the reason for the high T → T absorption intensity, we need to analyze the wave functions of the T_3 and T_2 states. Both states contain similar components of the single-electron excitations:

$$T_2 = 0.745\,(\text{HOMO} - \text{LUMO+1}) - 0.665\,(\text{HOMO−1} - \text{LUMO}) \quad (1)$$

$$T_3 = 0.666\,(\text{HOMO} - \text{LUMO+1}) + 0.746\,(\text{HOMO−1} - \text{LUMO}) \quad (2)$$

In eq 1, both single-electron excitations have opposite signs of transition dipole moment integrals and cancel each other. In eq 2, they contribute with the same signs and provide a strong T_1 → T_3 absorption. The characteristic mixture of triplet excitations in the TDDFT approach, eqs 1and 2, being

dx.doi.org/10.1021/jp4062576 | J. Phys. Chem. C XXXX, XXX, XXX−XXX

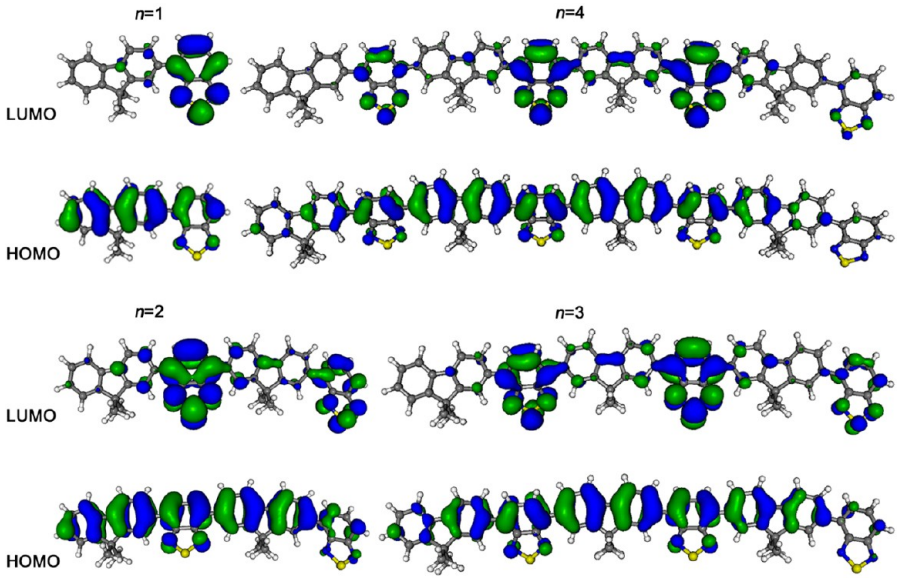

Figure 9. Contour plots of HOMO and LUMO orbitals of $(F8BT)_n$ (n = 1−4) oligomers.

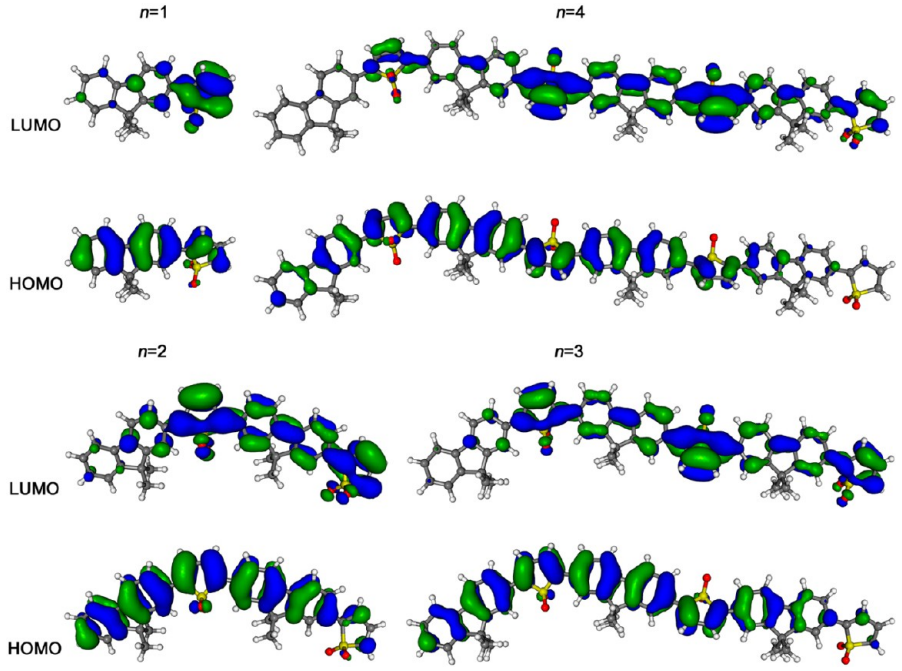

Figure 10. Contour plots of HOMO and LUMO orbitals of $(PFTSO2)_n$ (n = 1−4) oligomers.

responsible for the peculiarity of T−T absorption in the visible region of the PFP monomer, retains its orbital nature for higher copolymers.

The calculated S_0−T_1 transition energy of $(PFP)_2$ copolymer is 2.89 eV. The $T_1 \rightarrow T_2$ transition is predicted to be at 1271 nm (0.97 eV) with zero oscillator strength, and the $T_1 \rightarrow T_3$ transition is very intense (f = 2.89) and comes into the visible region with a longer wavelength (660 nm or 1.88 eV) than in the PFP monomer. The orbital natures of both triplet states are almost the same, as in eqs 1 and 2, in both $(PFP)_2$ and $(PFP)_3$. The oscillator strength for the $T_1 \rightarrow T_3$ transition increases along the series as 2.57, 2.89, and 3.73.

t7t8 In Tables 7 and 8, we present TDDFT results for the polymers studied for the $S_0 \rightarrow S_1$ band and the $T_1 \rightarrow T_n$ transient absorption, respectively. Calculations indicate that upon increasing the chain length, the absorption spectra of oligomers shift smoothly from UV to visible region. The first $S_0 \rightarrow S_1$ absorption band is the most intense in the spectra. The PM3 CI calculations show that its intensity almost saturates after n = 5.

The transient absorption spectra observed by pulse radiolysis of benzene solutions in the presence of triplet energy donors[12,15] are interpreted as due to the $T_1 \rightarrow T_n$ transitions (Table 8). The same type of T_1−T_n transitions, as with those for T_n states shown in eqs 1 and 2, have been obtained for all monomers and dimers, except the F8BT species. The $T_1 \rightarrow T_2$ transition is almost forbidden in all oligomers, and only the T_3 counterpart, eq 2, provides an intense transient absorption. A strong change in the calculated $T_1 \rightarrow T_3$ excitation energy is predicted upon dimerization for all species except PFPSO2.

dx.doi.org/10.1021/jp4062576 | J. Phys. Chem. C XXXX, XXX, XXX−XXX

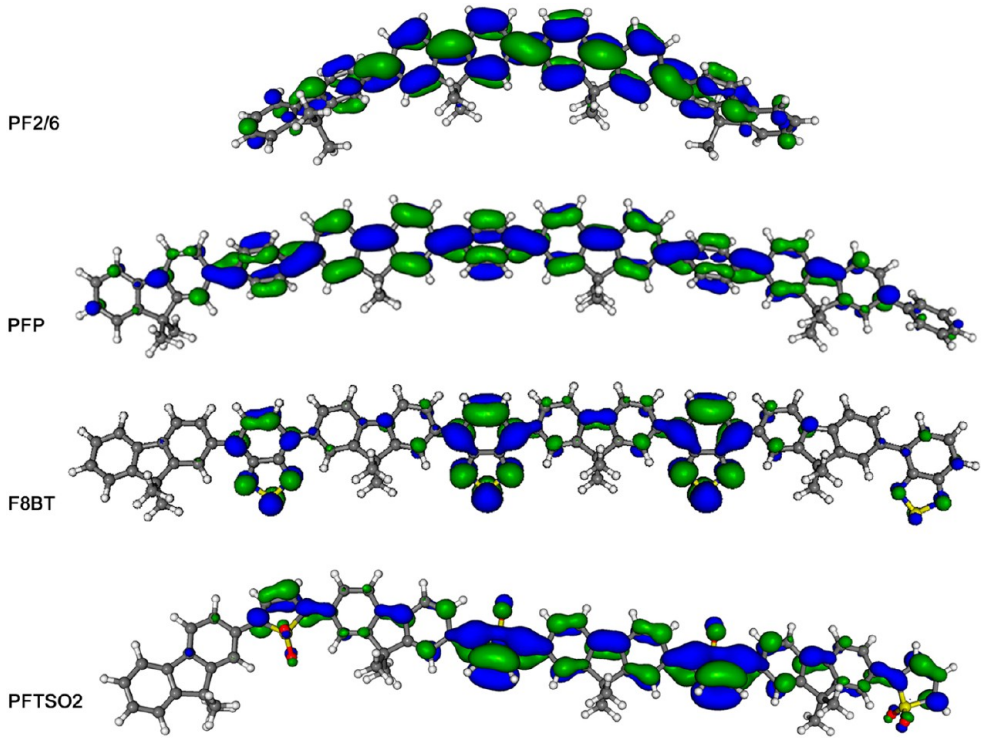

Figure 11. Contour plots of the LUMOs of the $(F2/6)_4$, $(PFP)_4$, $(F8BT)_4$, and $(PFTSO2)_4$ oligomers.

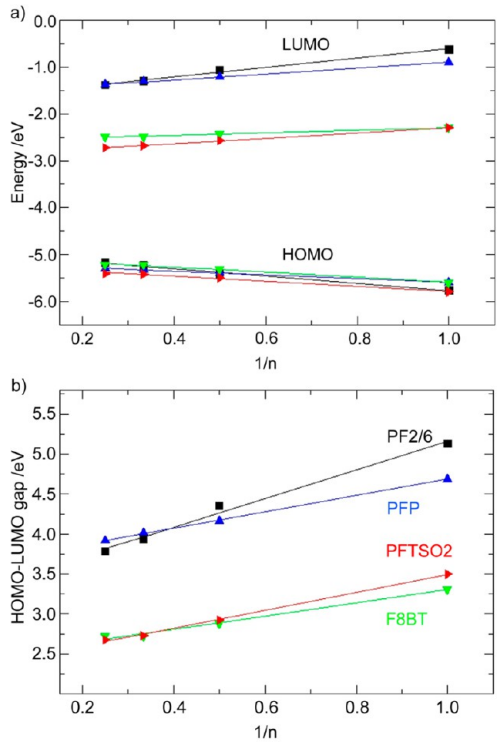

Figure 12. (a) B3LYP/3-21G* calculated HOMO and LUMO energies of PF2/6 (■), PFP (blue ▲), F8BT (green ▼), and PFTSO2 (red right triangles) oligomers as a function of the inverse number of monomer units. (b) HOMO−LUMO gaps as a function of reciprocal chain length n in the n = 1−4 oligomers of F2/6 (■), PFP (blue ▲), F8BT (green ▼), and PFTSO2 (red right triangles).

Geometry optimization of the T_1 state by the spin-unrestricted UB3LYP method indicates that the spin density in PFP trimer is localized in such a way that terminal rings do not bear nonpaired spins. This trend is seen even in the dimer. The spin-unrestricted PM3 calculations for the longer oligomers (n = 4−8) show that the triplet state spin density is localized inside the three-member chain moiety. This means that the T−T transition band is not shifted much for longer oligomers (n = 4−8). The above results imply that triplet excitation is slightly more localized (2−3 units) than the S_1 excitation. This is in agreement with experimental results on oligofluorenes[37,38] and polyfluorenes.[39] For all of the copolymers in these calculations, except PFTSO2, the T−T absorption maxima were observed by pulse radiolysis to be in the 730−760 nm region.[12,36] For the PFTSO2 polymer, only a weak absorption was observed around 580 nm.[12] These results correlate with our data for the monomer and dimer (Table 8) because the T−T transitions in PFTSO2 are rather weak; the result for trimer is highly uncertain because a number of low-intensity transitions are predicted and the correct choice is difficult here.

CONCLUSIONS

Three alternating 9,9-dialkylfluorene copolymers, having benzothiadiazole (F8BT), thiophene *S*,*S*-dioxide (PFTSO2), and phenylene (PFP) groups, have been studied by ^1H and ^{13}C NMR spectroscopy and density functional theory (DFT), and the behavior has been compared to that of the homopolymer poly[2,7-(9,9-bis(2′-ethylhexyl)-fluorene)] (PF2/6). While co-polymerization of 9,9-dialkylfluorene with the phenylene group does not significantly affect the electronic properties of PF2/6, the electron-accepting properties of F8BT and PFTSO2 are markedly improved, favoring application of these copolymers for electron injection in light emitting and other devices. In addition, time-dependent DFT has been used to obtain a better understanding of the character of selected excited states within the singlet and triplet state manifolds. Comparison with

dx.doi.org/10.1021/jp4062576 | J. Phys. Chem. C XXXX, XXX, XXX−XXX

Table 5. Values of the HOMO ($-\varepsilon_{HOMO}$) and LUMO Energies ($-\varepsilon_{LUMO}$), Relative to the Vacuum Level, and HOMO−LUMO Gaps (eV), Vertical Ionization Potentials,[a] and Vertical Electron Affinities (eV) of the Oligomers of This Study Calculated at the DFT B3LYP/3-21G* Level

oligomer	$-\varepsilon_{HOMO}$	$-\varepsilon_{LUMO}$	Δ_{H-L}	IP_v	EA_v
$(F2/6)_n$					
$n = 1$	5.76	0.63	5.13	7.50	−1.05
$n = 2$	5.42	1.06	4.35	6.68	−0.18
$n = 3$	5.23	1.30	3.93	6.28	0.26
$n = 4$	5.17	1.39	3.78	6.09	0.47
$n = \infty$[b]	4.98	1.62	3.37	5.67	0.91
$(PFP)_n$					
$n = 1$	5.59	0.90	4.69	7.05	−0.53
$n = 2$	5.38	1.22	4.16	6.45	0.16
$n = 3$	5.32	1.30	4.02	6.18	0.44
$n = 4$	5.30	1.38	3.92	6.03	0.61
$n = \infty$	5.19	1.52	3.67	5.73	0.95
$(F8BT)_n$					
$n = 1$	5.60	2.29	3.31	6.99	0.66
$n = 2$	5.31	2.43	2.88	6.32	1.35
$n = 3$	5.21	2.49	2.72	6.04	1.65
$n = 4$	5.21	2.49	2.72	5.89	1.80
$n = \infty$	5.05	2.57	2.48	5.56	2.15
$(PFTSO2)_n$					
$n = 1$	5.79	2.29	3.50	7.22	0.69
$n = 2$	5.49	2.56	2.93	6.54	1.49
$n = 3$	5.41	2.68	2.73	6.27	1.82
$n = 4$	5.40	2.72	2.68	6.14	1.98
$n = \infty$	5.24	2.86	2.38	5.80	2.38

[a]Vertical ionization potentials (IP_v) and vertical electronic affinities (EA_v) were calculated, respectively, as $IP_v = E_v(+1) - E(0)$ and $EA_v = E(0) - E_v(-1)$, where $E(0)$ is the ground-state energy of the neutral molecule and $E_v(+1)$ and $E_v(-1)$ are the energy of the radical cation and the energy of the radical anion, respectively, where the geometry was kept fixed in the neutral ground-state geometry. [b]$n = \infty$ IPs and EAs were extrapolated from the calculated values.

Table 6. Calculated Excitation Energies (eV) for a Series of the $(PFP)_n$ Oligomers in Comparison with Polymer Experimental Data

oligomer	S_0-T_1	T_1-T_2	T_1-T_3	S_0-S_1
$(PFP)_1$	3.10	0.99	2.77	4.20
$(PFP)_2$	2.89	0.97	1.88	3.53
$(PFP)_3$	2.81	0.97	1.50	3.34
exp.[a]	2.32	not observed	1.70	3.16

[a]Reference 12.

Table 7. Calculated $S_0 \rightarrow S_1$ Excitation Energies (eV) for a Series of Alternating Fluorene-Based Oligomers in Comparison with the Polymer Experimental Data

oligomer	monomer	dimer	trimer	exp.[a,b]
PFPSO2	4.10	3.49	2.28	2.39[a]
PFP	4.20	3.53	3.34	3.16[a]
F8BT	4.21	2.50	2.39	2.53[a]
F2/6	4.26	3.57	3.36	*a*

[a]Reference 12. [b]Reference 15.

580 literature electronic spectral data gives detailed insights into the
581 nature of the electronic transitions in these fluorene-based
582 conjugated copolymers.

Table 8. Calculated $T_1 \rightarrow T_n$ Excitation Energies (eV) for a Series of Alternating Fluorene-Based Oligomers in Comparison with the Polymer Transient Absorption Experimental Data

oligomer	monomer	dimer	trimer	exp.[a,b]
PFPSO2	2.85	2.47	1.54	2.14[a]
PFP	2.77	1.88	1.50	1.70[a,b]
F8BT	2.07	1.29	1.31	1.63[a]
F2/6	2.54	1.79	1.61	1.65[a,b]

[a]Reference 12. [b]Reference 36.

AUTHOR INFORMATION

583

Corresponding Author

584

*Tel.: +351-239-854453. Fax: +351-239-827703. E-mail: liciniaj@ci.uc.pt.

585 586

Notes

587

The authors declare no competing financial interest.

588

ACKNOWLEDGMENTS

589

L.L.G.J. thanks FCT of the Portuguese Ministry for Science, Technology and Higher Education, for the postdoctoral grant SFRH/BPD/26415/2006, the LCA of the Department of Physics of the University of Coimbra for the computing facilities (Milipeia Cluster), and the Rede Nacional de RMN (REDE/1517/RMN/2005), the Portuguese NMR Network, for spectrometer facilities. The Coimbra group is also grateful to the FCT for financial support (PEst-C/QUI/UI0313/2011). B.F.M. thanks the Ukrainian Ministry for Science and Education for a grant 0109U0002547. Parts of the computations were performed on resources provided by the Swedish National Infrastructure for Computing (SNIC) at the parallel computer centre (PDC), through the project "Multiphysics Modeling of Molecular Materials", SNIC 020/11-23. The work at IT was partially supported by FCT under contract PEst-OE/EEI/LA0008/2013.

590 591 592 593 594 595 596 597 598 599 600 601 602 603 604 605

REFERENCES

606

(1) Friend, R. H.; Gymer, R. W.; Holmes, A. B.; Burroughes, J. H.; Taliani, C.; Bradley, D. D. C.; Dos Santos, D. A.; Bredas, J. L.; Logdlund, M.; Salaneck, W. R. Electroluminescence in Conjugated Polymers. *Nature* **1999**, *397*, 121.

(2) Forrest, S. R. The Path to Ubiquitous and Low-Cost Organic Electronic Appliances on Plastic. *Nature* **2004**, *428*, 911−915.

(3) Pivrikas, A.; Sariciftci, N. S.; Juska, G.; Osterbacka, R. A Review of Charge Transport and Recombination in Polymer/Fullerene Organic Solar Cells. *Prog. Photovoltaics* **2007**, *15*, 677−696.

(4) See, for example: Bashir, T.; Fast, L.; Skrifvars, M.; Persson, N. K. Electrical Resistance Measurement Methods and Electrical Characterization of Poly(3,4-ethylenedioxythiophene)-Coated Conductive Fibers. *J. Appl. Polym. Sci.* **2012**, *124*, 2954−2961.

(5) Bernius, M.; Inbasekaran, M.; Woo, E.; Wu, W.; Wujkowski, L. Fluorene-Based Polymers-Preparation and Applications. *J. Mater. Sci.: Mater. Electron.* **2000**, *11*, 111−116.

(6) Leclerc, M. Polyfluorenes: Twenty Years of Progress. *J. Polym. Sci., Part A: Polym. Chem.* **2001**, *39*, 2867−2873.

(7) Scherf, U.; List, E. J. W. Semiconducting Polyfluorenes−Towards Reliable Structure−Property Relationships. *Adv. Mater.* **2002**, *14*, 477−487.

(8) Scherf, U. In *Polyfluorenes*; Neher, D., Ed.; Springer-Verlag: Berlin, Heidelberg, 2008.

(9) Yang, L.; Feng, J.-K.; Ren, A.-M.; Sun, J.-Z. The Electronic Structure and Optical Properties of Carbazole-Based Conjugated Oligomers and Polymers: A Theoretical Investigation. *Polymer* **2006**, *47*, 1397−1404.

607 608 609 610 611 612 613 614 615 616 617 618 619 620 621 622 623 624 625 626 627 628 629 630 631 632 633

dx.doi.org/10.1021/jp4062576 | J. Phys. Chem. C XXXX, XXX, XXX−XXX

(10) Yang, L.; Feng, J.-K.; Ren, A.-M. Theoretical Studies on the Electronic and Optical Properties of Two New Alternating Fluorene/Carbazole Copolymers. *J. Comput. Chem.* **2005**, *26*, 969−979.
(11) Yang, L.; Ren, A.-M.; Feng, J.-K.; Wang, J.-F. Theoretical Investigation of Optical and Electronic Property Modulations of π-Conjugated Polymers Based on the Electron-Rich 3,6-Dimethoxyfluorene Unit. *J. Org. Chem.* **2005**, *70*, 3009−3020.
(12) Fonseca, S. M.; Pina, J.; Arnaut, L. G.; Seixas de Melo, J.; Burrows, H. D.; Chattophadhyay, N.; Alcácer, L.; Charas, A.; Morgado, J.; Monkman, A. P.; Asawapirom, U.; Scherf, U.; Edge, R.; Navaratnam, S. Triplet-State and Singlet Oxygen Formation in Fluorene-Based Alternating Copolymers. *J. Phys. Chem. B* **2006**, *110*, 8278−8283.
(13) Charas, A.; Morgado, J.; Martinho, J. M. G.; Alcácer, L.; Lim, S. F.; Friend, R. H.; Cacialli, F. Synthesis and Luminescence Properties of Three Novel Polyfluorene Copolymers. *Polymer* **2003**, *44*, 1843.
(14) Jansson, E.; Jha, P. C.; Ågren, H. Chain Length Dependence of Singlet and Triplet Excited States of Oligofluorenes: A Density Functional Study. *Chem. Phys.* **2007**, *336*, 91−98.
(15) Fratiloiu, S.; Fonseca, S. M.; Grozema, F.; Burrows, C.; Costa, H. D.; Charas, M. L.; Morgado, A.; Siebbeles, J.; Opto-Electronic, L. D. A. Properties of Fluorene-Based Derivatives as Precursors for Light-Emitting Diodes. *J. Phys. Chem. C* **2007**, *111*, 5812−5820.
(16) Grell, M.; Knoll, W.; Lupo, D.; Meisel, A.; Miteva, T.; Neher, D.; Nothofer, H.-G.; Scherf, U.; Yasuda, A. Blue Polarized Electroluminescence from a Liquid Crystalline Polyfluorene. *Adv. Mater.* **1999**, *11*, 671−675.
(17) Knaapila, M.; Almásy, L.; Garamus, V. M.; Ramos, M. L.; Justino, L. L. G.; Galbrecht, F.; Preis, E.; Scherf, U.; Burrows, H. D.; Monkman, A. P. An Effect of Side Chain Length on the Solution Structure of Poly(9,9-dialkylfluorene)s in Toluene. *Polymer* **2008**, *49*, 2033−2038.
(18) Rahman, M. H.; Liao, S. C.; Chen, H.-L.; Chen, J. H.; Ivanov, V. A.; Chu, P. P. J.; Chen, S. A. Aggregation of Conjugated Polymers in Aromatic Solvent. *Langmuir* **2009**, *25*, 1667−1674.
(19) Schmidt, M. W.; Baldridge, K. K.; Boatz, J. A.; Elbert, S. T.; Gordon, M. S.; Jensen, J. H.; Koseki, S.; Matsunaga, N.; Nguyen, K. A.; Su, S. J.; Windus, T. L.; Dupuis, M.; Montgomery, J. A. General Atomic and Molecular Electronic Structure System. *J. Comput. Chem.* **1993**, *14*, 1347−1363.
(20) Becke, A. D. Density-Functional Thermochemistry. 3.The Role of Exact Exchange. *J. Chem. Phys.* **1993**, *98*, 5648−5652.
(21) Lee, C.; Yang, W.; Parr, R. G. Development of the Colle-Salvetti Correlation-Energy Formula into a Functional of the Electron-Density. *Phys. Rev. B* **1988**, *37*, 785−789.
(22) Kuhn, H. Free Electron Model for Absorption Spectra of Organic Dyes. *J. Chem. Phys.* **1948**, *16*, 840−841.
(23) Bylaska, E. J.; de Jong, W. A.; Govind, N.; Kowalski, K.; Straatsma, T. P.; Valiev, M.; Wang, D.; Apra, E.; Windus, T. L.; Hammond, J.; Nichols, P.; Hirata, S.; Hackler, M. T.; Zhao, Y.; Fan, P.-D.; Harrison, R. J.; Dupuis, M.; Smith, D. M. A.; Nieplocha, J., Tipparaju, V.; Krishnan, M.; Wu, Q.; Van Voorhis, T.; Auer, A. A.; Nooijen, M.; Brown, E.; Cisneros, G.; Fann, G. I.; Fruchtl, H.; Garza, J.; Hirao, K.; Kendall, R.; Nichols, J. A.; Tsemekhman, K.; Wolinski, K.; Anchell, J.; Bernholdt, D.; Borowski, P.; Clark, T.; Clerc, D.; Dachsel, H.; Deegan, M.; Dyall, K.; Elwood, D.; Glendening, E.; Gutowski, M.; Hess, A.; Jaffe, J.; Johnson, B.; Ju, J.; Kobayashi, R.; Kutteh, R.; Lin, Z.; Littlefield, R.; Long, X.; Meng, B.; Nakajima, T.; Niu, S.; Pollack, L.; Rosing, M.; Sandrone, G.; Stave, M.; Taylor, H.; Thomas, G.; van Lenthe, J.; Wong, A.; Zhang, Z. *NWChem, A Computational Chemistry Package for Parallel Computers, Version 5.1*; Pacific Northwest National Laboratory: Richland, WA, 2007. Kendall, R. A.; Apra, E.; Bernholdt, D. E.; Bylaska, E. J.; Dupuis, M.; Fann, G. I.; Harrison, R. J.; Ju, J.; Nichols, J. A.; Nieplocha, J.; Straatsma, T. P.; Windus, T. L.; Wong, A. T. High Performance Computational Chemistry: An Overview of NWChem a Distributed Parallel Application. *Comput. Phys. Commun.* **2000**, *128*, 260−283.
(24) Vahtras, O.; Ågren, H.; Jørgensen, P.; Jensen, H. J. A.; Helgaker, T.; Olsen, J. Multiconfigurational Quadratic Response Functions for Singlet and Triplet Perturbations: The Phosphorescence Lifetime of Formaldehyde. *J. Chem. Phys.* **1992**, *97*, 9178−9187.
(25) Luo, Y.; Jonsson, D.; Norman, P.; Ruud, K.; Vahtras, O.; Minaev, B.; Ågren, H.; Rizzo, A.; Mikkelsen, K. V. Some Recent Developments of High-Order Response Theory. *Int. J. Quantum Chem.* **1998**, *70*, 219−239.
(26) Stewart, J. J. P. Optimization of Parameters for Semiempirical Methods I. Method. *J. Comput. Chem.* **1989**, *10*, 209−220.
(27) Justino, L. L. G.; Ramos, M. L.; Abreu, P. E.; Carvalho, R. A.; Sobral, A. J. F. N.; Scherf, U.; Burrows, H. D. Conformational Studies of Poly(9,9-dialkylfluorene)s in Solution Using NMR Spectroscopy and Density Functional Theory Calculations. *J. Phys. Chem. B* **2009**, *113*, 11808−11821.
(28) Justino, L. L. G.; Ramos, M. L.; Knaapila, M.; Marques, A. T.; Kudla, C. J.; Scherf, U.; Almásy, L.; Schweins, R.; Burrows, H. D.; Monkman, A. P. Gel Formation and Interpolymer Alkyl Chain Interactions with Poly(9,9-dioctylfluorene-2,7-diyl) (PFO) in Toluene Solution: Results from NMR, SANS, DFT, and Semiempirical Calculations and Their Implications for PFO beta-Phase Formation. *Macromolecules* **2011**, *44*, 334−343.
(29) Pauling, L. The Diamagnetic Anisotropy of Aromatic Molecules. *J. Chem. Phys.* **1936**, *4*, 673−677.
(30) Lonsdale, K. Magnetic Anisotropy and Electronic Structure of Aromatic Molecules. *Proc. R. Soc. London* **1937**, *A159*, 149−170.
(31) London, F. Théorie quantique des courants interatomiques dans les combinaisons aromatiques. *J. Phys. Radium* **1937**, *8*, 397.
(32) Faglioni, F.; Ligabue, A.; Pelloni, S.; Soncini, A.; Viglioni, R. G.; Ferraro, M. B.; Zanasi, R.; Lazzeretti, P. Why Downfield Proton Chemical Shifts are not Reliable Aromaticity Indicators. *Org. Lett.* **2005**, *7*, 3457−3460.
(33) Belletête, M.; Beaypré, S.; Bouchard, J.; Blondin, P.; Leclerc, M.; Durocher, G. Theoretical and Experimental Investigations of the Spectroscopic and Photophysical Properties of Fluorene-phenylene and Fluorene-thiophene Derivatives: Precursors of Light-emitting Polymers. *J. Phys. Chem. B* **2000**, *104*, 9118−9125.
(34) Pal, B.; Yen, W.-C.; Yang, J.-S.; Chao, C.-Y.; Hung, Y.-C.; Lin, S.-T.; Chuang, C.-H.; Chen, C.-W.; Su, W.-F. Substituent Effect on the Optoelectronic Properties of Alternating Fluorene-Cyclopentadithiophene Copolymers. *Macromolecules* **2008**, *41*, 6664−6671.
(35) Schwenn, P. E.; Burn, P. L.; Powell, B. J. Calculation of Solid State Molecular Ionization Energies and Electron Affinities for Organic Semiconductors. *Org. Electron.* **2011**, *12*, 394−403.
(36) Monkman, A. P.; Burrows, A. D.; Hartwell, L. J.; Horsburg, I. E.; Hamblett, I.; Navaratnam, S. Triplet Energies of Pi-Conjugated Polymers. *Phys. Rev. Lett.* **2001**, *86*, 1358−1361.
(37) Wasserberg, F.; Dudek, S. P.; Meskers, S. C. J.; Janssen, R. A. J. Comparison of the Chain Length Dependence of the Singlet- and Triplet-Excited States of Oligofluorenes. *Chem. Phys. Lett.* **2005**, *411*, 273−277.
(38) Chi, C. Y.; Im, C.; Wegner, G. Lifetime Determination of Fluorescence and Phosphorescence of a Series of Oligofluorenes. *J. Chem. Phys.* **2006**, *124*, 024907.
(39) King, S. M.; Vaughan, H. L.; Monkman, A. P. Orientation of Triplet and Singlet Transition Dipole Moments in Polyfluorene, Studied by Polarized Spectroscopies. *Chem. Phys. Lett.* **2007**, *440*, 268−272.